RILEM Technical Letters (2025) 10: 98-105
https://doi.org/10.21809/rilemtechlett.2025.224

Strain-level dependency in static and dynamic Young's moduli characterisation of hydraulic lime mortars

Marialuigia Sangirardi[1,*], Miles R. W. Judd[1], Anil Ozdemir[1,2], Sinan Acikgoz[1]

[1]Department of Engineering Science, University of Oxford, United Kingdom
[2]Department of Civil Engineering, Gazi University, Turkiye

Received: 06 August 2025 / Accepted: 10 December 2025 / Published online: 16 December 2025

Abstract

Young's modulus is commonly estimated using dynamic tests or from load and deformation measurements under static loading. However, these methods may yield different results due to variations in strain levels where characterisation is conducted. Existing studies reported discrepancies between static and dynamic Young's moduli of hydraulic lime mortar. This paper examines the role that strain amplitudes and testing configurations play during Young's moduli characterisation of prismatic samples to understand the root causes for these differences. Dynamic characterisation is conducted using standard impulse excitation of vibration tests while static characterisation is done with three-point bending and uniaxial compression tests. A tailored loading regime is used to examine the evolution of Young's modulus at different strain levels. Repeated IEV measurements reveal progressive decay with increasing strain amplitudes. A similar trend is observed for static moduli, although decay magnitudes are notably higher and depend on the adopted test configuration. Reductions in Young's moduli are associated with microscale damage processes and were observed at strain levels as low as 100 με. They become notably pronounced at compressive loads corresponding to ~30% of material compressive strength, which is typically used for static elasticity characterisation. The results highlight the small-strain nonlinearity of hydraulic lime mortar and indicate the need for improved characterisation procedures to describe the constitutive behaviour of this material.

Keywords: Young's modulus; Hydraulic lime mortar; Strain-dependency; Digital image correlation (DIC); Material characterisation.

1 Introduction

Young's modulus quantifies material stiffness, and it can be determined through both static and dynamic testing methods. For hydraulic lime mortar, Young's modulus determination is not standardised by specialised codes. Consequently, guidelines originally developed for other materials are adopted, where the underlying assumptions may be different. The main ambiguity lies in the definition of Young's modulus (Fig.1a). Should this parameter refer to tangent or secant quantities? What strain level is appropriate for characterisation? Should the Young's modulus be calculated using data from the loading or unloading branches?

Standardised approaches offer different answers to these questions. Static methods derive Young's modulus from the average stress and average strain response measured under monotonically increasing compressive loads at strain rates of 10^{-6}-10^{-4} s^{-1}. While the loads are applied cyclically to stabilise the measurements, the interpretation of Young's modulus neglects any potential plastic strain accumulation during cycling. EN 14580-2005 [1] defines the static modulus of natural stone samples under compression as the secant modulus between 2% and 33% of the mean compressive strength (f_c). In contrast, EN 12390-13 [2] defines E_s as the secant modulus of concrete between 10-20% and 33% of f_c. Assuming a ratio of Young's modulus to compressive strength of 1/1000, strain magnitudes in the static characterisation tests are estimated to be in the order of 100$\mu\varepsilon$.

Dynamic methods estimate Young's modulus from wave velocities or resonant frequencies. The latter approach is less sensitive to errors caused by voids, and will be examined in this study. Either impulsive loads or continuous excitations are used during resonant frequency tests (see EN 1881-209:1990 [3] and EN 14146:2004 [4]). In the more commonly used impulse excitation of vibration (IEV) tests (standardised in ASTM E1876-22 [5]), resonant frequencies of beam-like samples are measured after they are gently struck by a hammer. The identified frequencies are then used to compute the material Young's modulus and Poisson's ratio

*Corresponding author: Marialuigia Sangirardi, E-mail: marialuigia.sangirardi@eng.ox.ac.uk

via Timoshenko beam theory. In a previous study, it was estimated that hydraulic lime mortar samples experienced maximum strains in the range 1-10$\mu\varepsilon$ during IEV tests [6]; this corresponds to maximum strain rates in the order of 10^{-3}-10^{-2} s^{-1}. While the reported strain magnitudes and rates may vary according to the impulsive forces applied on the sample, these variations were observed to be minor for a given setup and operator.

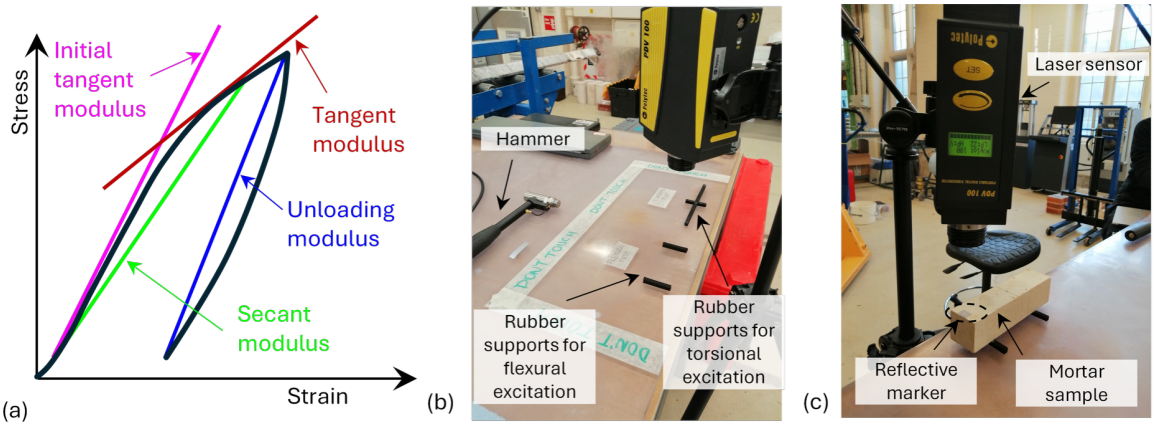

Figure 1. (a) Diagrammatic representation of a stress-strain curve for lime mortar in compression and different definitions of the static elastic modulus (adapted from [14]), (b) IEV setup details, (c) mortar sample subjected to IEV test in flexural configuration.

From the foregoing discussions, it is clear that the adopted strain levels and rates are notably different in static and dynamic characterisation approaches. On the one hand, larger strain levels may lead to damage in the material and influence characterisation results. A previous study [7] demonstrates notable plastic strain accumulation in hydraulic lime mortars at low compressive stresses, which suggests that strain levels may strongly influence Young's modulus estimations. On the other hand, strain rate effects (arising due to the incompressibility of free water, viscosity of binder phases and the rate-dependent debonding of aggregates) may also have an impact. The data in [8] suggests that compressive strength may increase by ~20% in hydraulic lime mortars when average strain rates rise from ~10^{-6} to 10^{-4} s^{-1}. Another study [9] notes 20% dynamic increase in flexural strength for increased strain rates up to ~10^{-3}-10^{-2} s^{-1}. Contrary to strength increases at high speeds, a study on lime-cement mortars [10] noted a consistent reduction of Young's modulus with increasing strain rates. In addition to these factors, it should be noted that both loading and unloading moduli influence the characterisation during IEV tests; this is different from static tests where only loading moduli are investigated.

Due to the outlined discrepancies, static and dynamic Young's moduli may differ significantly [11,12]. The differences are minor for concrete materials [13,14], and various linear relationships have been found to relate the two parameters for natural stones [15,16]. In contrast, the few studies investigating hydraulic lime mortars do not indicate a consistent relationship between these parameters: reported static-to-dynamic modulus ratios (E_{st}/E_{dyn}) vary from 0.625-0.676 [17] to 0.77-0.95 [18]. To demonstrate the engineering significance of these ratios, the Young's modulus of St Astier NHL 3.5 mortar (the one used in this study) may be considered. According to the manufacturer's technical sheet, the dynamic Young's modulus is 9000 MPa (determined using ultrasonic pulse velocity tests after 28 days curing for a 1:2.5 (lime:sand) volume mix ratio [19]). Considering the lower-bound E_{st}/E_{dyn} ratio of 0.625 from the literature, the corresponding static Young's modulus would be 5625 MPa. This static value is lower than the brick Young's moduli examined in [6], while the dynamic value is considerably higher. These simple calculations highlight that drastic behavioural differences may be expected (e.g. spanning from strong mortar-weak brick behaviour to weak mortar-strong brick behaviour [20]) depending on the Young's modulus estimate adopted for the analyses.

The novel contribution of this paper is to address the relationship between the static and dynamic Young's moduli systematically at different strain levels. Whilst strain rate effects are not directly examined, the investigation also provides new insight into the role of this aspect. The investigation is done by conducting dynamic and static characterisation sequentially on the same samples. A slender rectangular prism test geometry, ordinarily used in standard three-point bending (3PB) tests [21], is chosen for this purpose. The 3PB configuration is first examined to characterise Young's modulus dynamically and then statically at low-strain magnitudes [6]. Then, a second set of samples is subjected sequentially to dynamic tests in the beam configuration and static tests under compression. The use of this geometry for static characterisation has already been examined in other studies (e.g. [18]) and is compliant with EN 14146:2004 [4]. Throughout the experiments, stereo Digital Image Correlation (DIC) is employed on sample surfaces to obtain the displacement and strain measurements required for static Young's modulus characterisation.

The paper is organised as follows: Section 2 describes the sample production and experimental setups. Section 3 presents and discusses the results obtained from the experiments. Finally, conclusions are drawn in Section 4.

2 Sample production and experimental setup

Six hydraulic lime mortar samples (40 mm × 40 mm × 160 mm) were prepared using St Astier NHL 3.5 lime and

Morestead sand in a 1:2.5 weight ratio. The water content during mixing was set to 20% of the combined weight of lime and sand, ensuring workable mortars with flow values in the range 180-187mm [6]. Specimens were cast in three separate batches numbered from 1 to 3. They were then cured for a total of sixty days: three days in the mould at 95% (±5%) humidity, four days outside the moulds at 95% (± 5%) humidity and fifty-three days under standard laboratory conditions (with a temperature of 19 ± 2°C, relative humidity of 50 ± 4% and CO_2 levels ranging from 400 to 900 ppm). The samples were divided into two groups named B (indicating specimens tested in bending configuration) and C (indicating specimens subjected to compression), with each group containing one specimen from each batch.

The dynamic elastic moduli of all specimens were determined via IEV, using the experimental setup presented in [6] and illustrated in Figs. 1b and c. The method consists of impulsive excitation of the sample under two different boundary conditions, which promote flexural and torsional vibrations. These boundary conditions are realised by placing the sample on compliant rubber strips of specific shapes affixed to an underlying rigid surface (Fig. 1b). Small reflective patches are affixed to the sample at designated locations to conduct velocity measurements with a digital laser vibrometer (Polytec PDV-100) (Fig. 1c). Velocity response of the sample during and after impact is recorded at 22kHz sampling rate. The data is post-processed to derive the lowest flexural and torsional frequencies from frequency peaks in the discrete Fast Fourier Transform (FFT) of the measured signal. The tests are repeated six times by the same operator, and the frequencies determined from the repeated tests are averaged. To ensure consistent strain levels, only 1% deviation was allowed from one frequency measurement to another. Otherwise, the tests were repeated. This approach resulted in small coefficients of variation for peak signal velocity (in the range 6-12%). Once the flexural and torsional frequencies are determined, the Young's modulus and Poisson's ratio are calculated via the iterative procedure described in ASTM E1876 [5] using the averaged frequencies as input.

To evaluate elastic behaviour under different strain regimes for different static testing arrangements, Group B samples were subjected to 3PB tests (Fig. 2a) while Group C samples were tested under uniaxial compression along their length (Fig. 2b). The test procedure for Group B samples follows EN 1015 [21]; displacement is controlled at a constant rate of 2μm/s, resulting in sample failure after 60 to 90 seconds. The tests were conducted using an Instron 5582 universal testing machine. A steel loading device was used to promote uniform distribution of forces at contacts, as described in [6]. The static Young's modulus $E_{s,3PB}$ is determined using the following expression:

$$E_{s,3PB} = \frac{F}{\Delta}\left(\frac{L^3}{4bh^3} + \frac{3L(1+\nu)}{5bh}\right) \quad (1)$$

where F and L represent the force read by the load-cell and the distance between the two lower supports (100mm), respectively. The sample cross-section had equal width and height (b = h = 40mm), and the Poisson's ratio v was assumed to be equal to 0.2 (varying this value from 0.1 to 0.3 produces a difference of only 5% in the calculated $E_{s,3PB}$ values). Midpoint deflection Δ was derived from neutral-axis displacements v measured at supports (points 1 and 3) and at midspan (point 2), as illustrated in Fig. 2a, according to the following expression:

$$\Delta = v_2 - \frac{v_3 + v_1}{2} \quad (2)$$

To minimise the influence of measurement noise on the static Young's modulus, the ratio F/Δ in Equation (1) is determined from the slope of the line fitted to the force and deflection measurements. This is done for loads between 10% (to provide enough measurement points for fitting) and 90% of the maximum force (to exclude datapoints corresponding to fracture initiation processes). To quantify the strain level during characterisation, the maximum axial strain in the beam for a given force can be calculated from the following expression:

$$\varepsilon_{\max} = \frac{3FL}{2E_{s,3PB}bh^2} \quad (3)$$

Slender prisms in Group C were subjected to uniaxial compression under force control. The testing machine (CONTROLS 65-L28Z10) has a rigid steel loading base plate and an adjustable upper steel plate (fixed during loading) mounted on a ball bearing to compensate for non-parallel contact surfaces. The static Young's modulus was determined from the average stress-strain response. The average strains were measured with six virtual extensometers (three on the front and three on the back surfaces of the specimen), following a similar procedure to the one suggested in EN 12390-13 [2].

Fig. 3 presents the loading path adopted for Group C samples, with loads expressed as a portion of the nominal compressive strength (f_c). After dynamic characterisation (IEV1), samples are placed in the test machine and preloaded to approximately 200N (Stage A). Then, loads are applied with a constant loading/unloading rate of 0.0125 MPa/s, with load plateaus of 10s duration introduced at specific stress levels, to facilitate the stabilisation of load and strain readings. The first six load plateaus are at stress levels of 0.05 f_c and 0.1 f_c, where the samples are cyclically loaded and unloaded (Stages B_1, C_1, B_2, C_2, B_3 and C_3). This cyclic loading procedure is inspired by EN 12390-13 [2] and aims to foster a more uniform contact between the sample and the load platens. Then, the specimen is completely unloaded and removed from the test machine to conduct dynamic characterisation (Stage IEV2). After this, the specimen is placed again in the test machine, preloaded, and a similar procedure of loading and unloading is conducted for load levels 0.3 f_c (thrice to assess repeatability), 0.5 f_c and 0.75 f_c. After each complete unloading, the dynamic Young's modulus of the sample is characterised via IEV tests (e.g. IEV3-6). Static Young's moduli are determined as secant moduli between two specified stages.

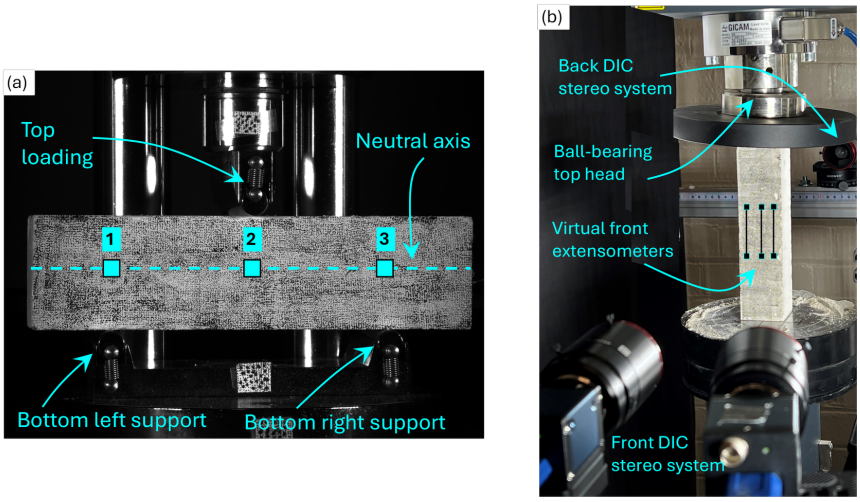

Figure 2. Test setup for (a) three-point bending test and (b) prism compression test.

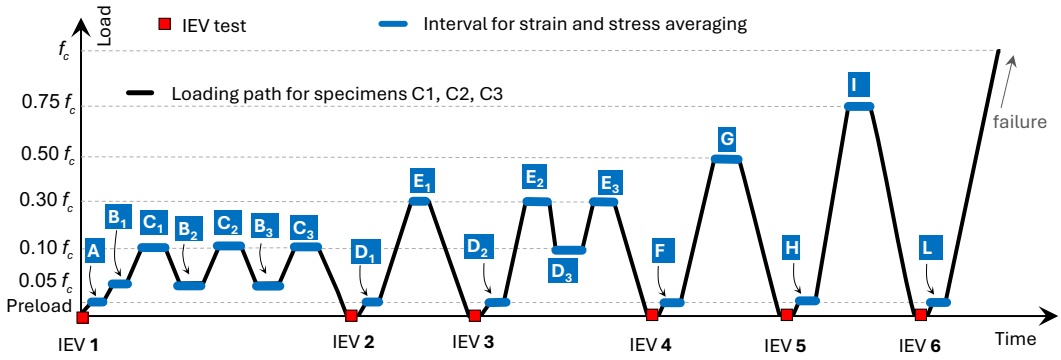

Figure 3. Loading path for sample group C, highlighting IEV test instances and image averaging plateaus.

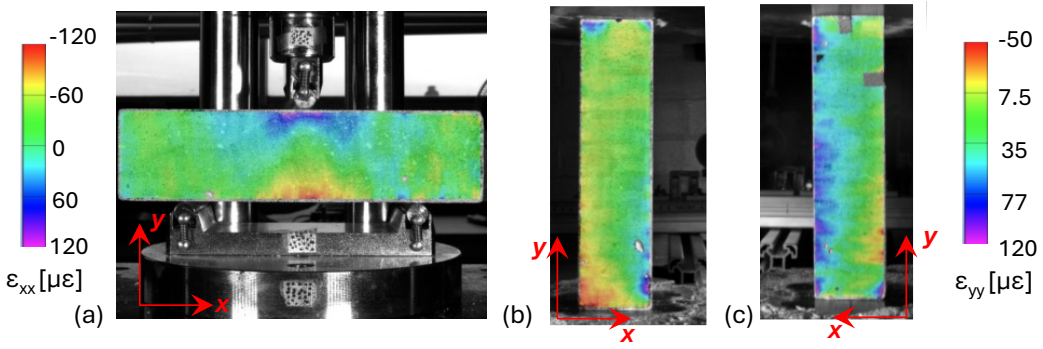

Figure 4. (a) horizontal strain map in three-point-bending test on specimen B1 when maximum axial strain reaches 120με, (b) vertical strain map on the front face of specimen C1 and (c) vertical strain map on the back face of specimen C1 at stage C_3 of the loading path.

Values of f_c were required to set the load levels for Group C tests. These were determined for each batch (1, 2, and 3) as the average of compression tests on two half-prisms (named a and b) obtained after fracture in 3PB tests following BS EN 1015-11 [21]. Due to the slender specimen geometry, the compressive strength exhibited by prisms is expected to be lower than the values measured for half prisms. Nonetheless, in the absence of specific pre-tests on prisms compressed along their length, the f_c estimate from half-prisms was considered the most appropriate option to set the load thresholds. The resulting values for f_c are 3.40MPa for Sample B1a-b, 3.83MPa for Sample B2a-b and 5.33MPa for Sample B3a-b.

The stereo-DIC system used to monitor surface deformations during 3PB and compression tests consisted of monochrome 26 MP cameras (Daheng ME2P-2621-15U3M) with 8-bit pixel depth (two in 3PB and four in compression tests), fitted with 25mm focal length lenses (Kowa LM25FC24M). For the 3PB tests, deflection was calculated by averaging ca. 250 displacement measurements (corresponding to an area of around 10 mm^2) at three locations along the neutral axis (shown in Fig. 2a), using a subset size of 21 pixels (≈ 0.8mm) and a step size of 5 pixels (≈ 0.2mm). The spatial averaging enabled improved displacement resolutions around 1μm. In this case, displacement measurements were only conducted on the front surface of the specimen; previous investigations

demonstrate that this one-sided setup is sufficient for accurate characterisation [6]. Although full-field strain measurements are not used for characterisation, horizontal strain fields are plotted in Fig. 4a to illustrate the expected beam behaviour; the highest tensile and compressive strains appear at mid-span, at the top and bottom parts of the sample, respectively. For convenience, a compression positive strain convention is adopted in this paper.

In uniaxial compression tests, virtual extensometers of 40 mm length were placed centrally on both the front and the back surfaces (Fig. 2b). Images obtained at load plateaus (see Fig. 3) were averaged to reduce measurement noise. Gauge point displacements were measured using a subset size of 27 pixels (≈1.1mm). Based on static images taken before preloading, a strain resolution of ≈10-30$\mu\varepsilon$ is expected after noise reduction via image averaging. The mean of all extensometer readings was then computed to determine axial shortening and average strain; this approach mitigates errors arising from both specimen misalignment (caused by non-central positioning) and contact load eccentricity [22]. Figs. 4b and c exemplify how vertical strain fields in the front and back of the sample vary due to these factors. These figures show sample response at the Stage C_3 of the loading path depicted in Fig.3. The maximum strain (with respect to preload Stage A) reaches approximately 120$\mu\varepsilon$, but compressive strains are higher for larger values of x coordinates and on the back of the specimen, because of non-uniform loading.

3 Results and discussion

3.1 Three-point bending test results

Estimates of the static Young's modulus from 3PB tests are reported first. Fig. 5a depicts the load-midspan deflection curves for the three specimens from group B. The experimental response is similar for specimens B1 and B3 (especially in the first half of the test), while specimen B2 shows lower stiffness from early load stages. This trend is also evident in Fig. 5b, which illustrates the evolution of the static modulus with increasing maximum strain levels.In Fig. 5b, values of $E_{d,IEV}$ are also reported with dotted straight lines.

A decrease in the static Young's Modulus is consistently observed, varying from 12% to 25% for the three samples from ~100 to ~300$\mu\varepsilon$. The maximum axial strains reported in the figure are calculated indirectly from beam theory (Equation 3). This approach may lead to incorrect estimates, especially at the initial stage of loading, when beam behaviour is not established due to imperfect contact. The unexpected minor stiffness increase in specimen B2 (see Fig. 5b) may be due to this reason. Beam theory (and the strain measurements in Fig. 4a) indicates that only a small part of the beam experiences high strain levels; this aspect should be considered when comparing strain-dependent decay of the Young's modulus from bending and compression tests. In this study, the value of $E_{s,3PB}$ is conventionally defined as the Young's modulus calculated when maximum axial strain reaches 100$\mu\varepsilon$. The resultant values are reported in Table 2.

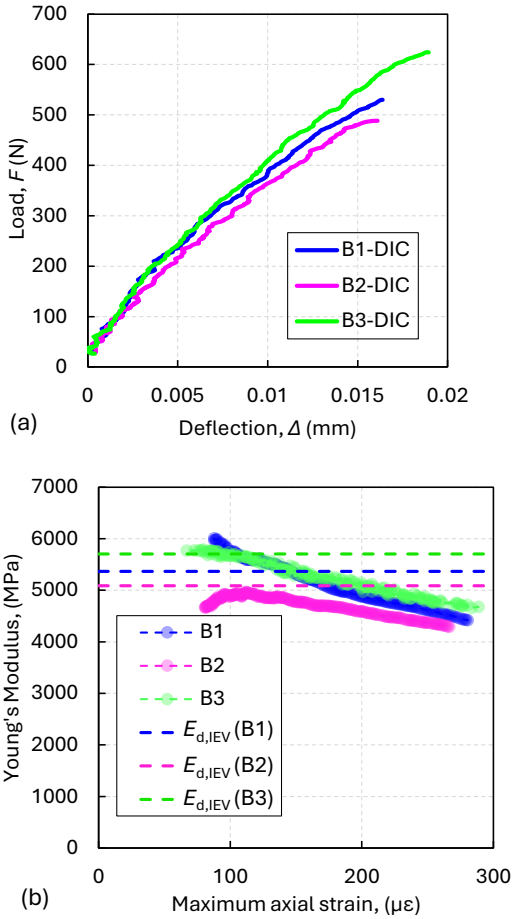

Figure 5. (a) load-deflection curves measured through DIC, and (b) Young's modulus evolution with maximum axial strain (calculated from DIC deflection and beam theory).

3.2 Compression test results

Fig. 6 reports the average stress-strain curve up to point E_3 and a summary of the $E_{s,c}$ values calculated on each loading branch, together with relevant $E_{d,IEV}$ results. The static modulus (calculated as the secant value) first decreases from branch A-B_1 to B_1-C_1 by approximately 18% and remains stable in branches B_2-C_2 and B_3-C_3. Only a small corresponding decrease of 0.4% is observed from IEV1 to IEV2. When loading between points D_1 and E_1 (30% of f_c), the specimen exhibits a 32.9% lower $E_{s,c}$ with respect to the initial value from A-B_1. The value of $E_{s,c}$ further decreases in branch D_2-E_2, indicating ongoing microstructural damage processes. The dynamic moduli measured after loading to point E_1 (IEV3) and after loading to E_3 (IEV4), show a consistent 3.5-4.5% decrease. A key observation from Fig. 6 is that the upper threshold of ~30 % f_c, commonly adopted for concrete and natural stone samples to characterise elastic response, may not be appropriate for hydraulic lime mortar due to damage accumulation.

Conducting a secant calculation for branch D_3–E_3, where the sample is loaded from a level of 10% f_c at D_3 to 30 % f_c at E_3 (Fig. 3), a higher $E_{s,c}$ is obtained. It results from a bottom threshold different from the previously adopted one (5% f_c). This is a commonly observed behaviour due to the stiff

unloading-reloading response and associated higher modulus (see Fig.1), which is distinct from the initial one due to damage accumulation. A similar behaviour was noted in an earlier study by [7] where changes in the loading and unloading moduli were evaluated within the framework of hardening plasticity [23].

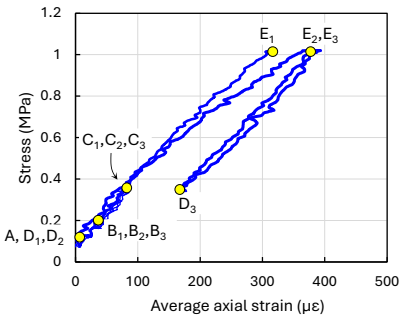

Load branch	$E_{s,c}$ (MPa)
$E_{d,IEV1}$ = 5477 MPa	
A-B_1	4550
B_1-C_1	3718
B_2-C_2	3889
B_3-C_3	3765
$E_{d,IEV2}$ = 5456 MPa	
D_1-E_1	3049
$E_{d,IEV3}$ = 5268 MPa	
D_2-E_2	2463
D_3-E_3	3045
$E_{d,IEV4}$ = 5021 MPa	

Figure 6. Stress-strain curve for specimen C1 up to point E_3 and values of the static and dynamic moduli.

The evolution (from instance IEV1 to IEV6) of the dynamic modulus of elasticity $E_{d,IEV}$ with further loading is reported in Fig. 7a, where the values measured on specimens from Group B are also plotted. The dynamic modulus is in the range of 5000–6000 MPa before loading, and consistent within each batch. Like earlier observations on sample C1 in Fig. 6, the first loading cycles have little effect on $E_{d,IEV}$, while cycles at higher stress levels result in progressive reduction of the measured dynamic modulus. This change is attributed to the accumulation of damage. Further circumstantial evidence of this hypothesis can be obtained by inspecting the modal damping ratios. This was done by fitting a single degree of freedom impulse response spectra to the IEV flexural test frequency response curves. This approach demonstrated increasing damping ratios, likely due to damage accumulation. For example, for sample C1, the damping ratios were identified throughout the test as 0.96% (IEV0), 1.03% (IEV1), 1.25% (IEV2), 1.27% (IEV3), 1.42% (IEV4) and 1.47% (IEV5).

The $E_{s,c}$ evolution is reported in Fig. 7b. This parameter refers to the secant modulus between the highlighted loading plateaus in Fig. 3, reported on the x-axis of the plot. Similarly to E_d, static $E_{s,c}$ values show a decreasing trend. However, the static secant moduli are notably lower than their dynamic counterparts and exhibit a more pronounced reduction. In the same graph, red symbols are used to indicate the maximum average strain reached by the specimen for a given specific secant $E_{s,c}$ calculation (i.e. the value reached on the higher load plateau of the interval). It is worth clarifying that the maximum strain observed in specimens C1, C2, and C3 for the same load step (e.g. HI) varies due to differences in both the applied stress levels (relative to their compressive strengths) and material variability. For instance, at stage I, the load applied to specimen C1 is 2.55 MPa, whereas specimen C2 is subjected to 2.87 MPa. Despite the relatively small difference in applied load, the maximum strain in C2 is nearly twice that of C1.

The full list of identified material properties is reported in Table 2, together with significant ratios of static and dynamic moduli. As expected, $E_{s,3PB}$ is close to the initial value of the dynamic modulus $E_{d,IEV}$. The $E_{s,3PB}/E_{d,IEV}$ ratio obtained for specimen B1is equal to 1.07. Since values greater than one are not realistic, this is a result of inaccuracies in either E_s or E_d calculation. The static modulus obtained from uniaxial compression tests at low strains ($E_{s,c}(AB_1)$) is, on average, approximately 20% lower than the corresponding dynamic values, resulting in $E_{s,c}(AB_1)/E_{d,IEV}$ ratios varying between 0.70 and 0.83. For higher strain levels (intervals D_1E_1 and FG), the static modulus decreases to about half of the initial dynamic modulus. Notably, the coefficient of variation (CoV) of this ratio also decreases as the influence of measurement noise diminishes with increasing strain magnitudes.

The analysis of the results in Table 2 reveals that, for comparable maximum strain levels in the range of approximately 100–150$\mu\varepsilon$, the modulus of elasticity determined from bending tests ($E_{s,3PB}$) is generally higher than that obtained from compression tests ($E_{s,c}(AB_1)$). This discrepancy is likely attributable to the different distributions of axial strain in the two loading configurations, as illustrated in Fig. 4. In 3PB, strain varies quasi-linearly across the specimen height, reaching peak values at the extreme fibres, while the rest of the section experiences lower strain. In contrast, axial compression produces more uniform strain distributions across the cross-section, with minor variations due to misalignment.

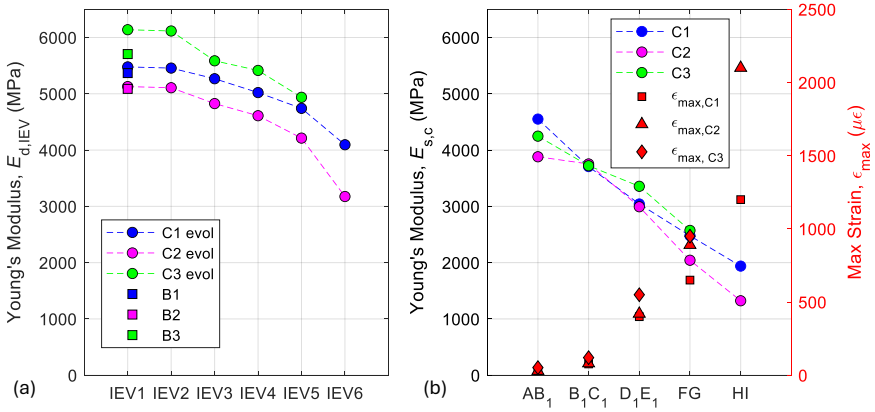

Figure 7. (a) Progression of the IEV-based dynamic elasticity modulus. (b) Progression of the extensometer-based static elastic modulus for different load cycles, as well as the corresponding strain levels.

Table 1. Overview of the identified static and dynamic moduli and relevant ratios.

Specimen	$E_{d,IEV}$*	$E_{s,3PB}$	$E_{s,c}(AB_1)$	$E_{s,c}(D_1E_1)$	$E_{s,c}(FG)$	$E_{s,f}/E_{d,IEV}$	$E_{s,c}(AB_1)/E_{d,IEV}$	$E_{s,c}(D_1E_1)/E_{d,IEV}$	$E_{s,c}(FG)/E_{d,IEV}$
B1	5368	5754				1.07			
C1	5453		4550	3049	2477		0.83	0.56	0.45
B2	5087	4941				0.97			
C2	5145		3881	2993	2043		0.75	0.58	0.40
B3	5706	5685				1.00			
C3	6075		4247	3356	2573		0.70	0.55	0.42
mean	5472	5460	4226	3133	2364	1.01	0.76	0.56	0.42
CoV (%)	6.8	8.3	7.9	6.2	11.9	5.2	8.9	2.7	6.7
Note *: This is the initial $E_{d,IEV}$ before any static test is conducted.									

4 Conclusions

This study systematically evaluates the influence of test configuration (e.g. three-point bending or compression) and strain levels during characterisation of the Young's modulus of hydraulic lime mortar. Dynamic moduli were obtained using impulse excitation of vibration measurements conducted prior to loading and at pre-determined intervals throughout the compression loading path. From stereo DIC measurements, static moduli were derived in the context of three-point bending and uniaxial compression tests, using displacements and strains measured directly on the specimen surface.

The results reveal reasonable agreement between static and dynamic modulus values at low strain levels. The ratio between static and dynamic modulus is approximately equal to 1 in bending tests (where maximum strain levels are approximately equal to 100$\mu\varepsilon$); this indicates that strain rate effects may not have a significant influence. In contrast, the ratio between static and dynamic modulus is 0.76 in comparable uniaxial compression tests (referring to $E_{st,c}(AB_1)$ where maximum average strain is approximately equal to 100$\mu\varepsilon$). The lower Young's moduli obtained from compression tests are attributed to the relative uniformity of strain fields in this testing configuration. While bending-induced strains concentrate in the extreme fibres of the samples, compression tests distribute strains more evenly, leading to the initiation of irreversible damage processes (i.e. microcracking in the binder matrix or at the sand-matrix interface). This aspect leads to more rapid reductions in the measured static moduli when uniaxial compression is adopted as the test configuration for characterisation.

In general, as characterisation strain levels are increased, the static moduli of hydraulic lime mortar progressively decrease. This was observed both for the bending and compression test configurations. Here, the characterisation results for samples placed under compression with loads corresponding to ~30% of the compressive strength are of particular interest, since this represents the load used to characterise elasticity in concrete and natural stone materials. Experimental evidence presented in this paper indicates that this level of loading induces significant irreversible damage in the material, leading to differences between stiffness estimates obtained during different parts of the load cycling. The samples are placed under ~500$\mu\varepsilon$ at this stage; for this strain level, the secant static modulus of hydraulic lime mortar is 30% less than its initial static value (characterised at ~100$\mu\varepsilon$ average strain). A more significant reduction in static modulus (≈ -60% from initial values) can be detected at maximum strains of ≈1500$\mu\varepsilon$. It is noteworthy that intermittent measurements of dynamic moduli (carried out by unloading the sample, after loading it to a specified stress/strain level) confirm the loss of stiffness, with reduced $E_{d,IEV}$ values. However, the decrease in the dynamic moduli is more gradual. This is expected as $E_{d,IEV}$ is influenced by the stiff unloading moduli of the material.

This study identifies the nonlinear small-strain behaviour of hydraulic lime mortar as the key reason for the large discrepancies between Young's moduli determined from standard static and dynamic test procedures. This finding emphasises the need to develop new testing protocols, particularly for static characterisation. In these protocols, a monotonic loading regime may be used instead of cycles to simplify secant Young's modulus calculations. In addition, target strain levels for characterisation may be defined depending on the strains that the material is likely to experience in-situ. Alternatively, simple constitutive laws (e.g. hardening plasticity type models in [23] can be calibrated using 1D axial stress- strain monotonic loading curves obtained from the tests. If this approach is taken, the secant elastic modulus should be defined at the smallest possible strain levels, dependent on the measurement noise. In this paper, the smallest loads that could be considered for secant calculations corresponded to between 5 and 10 % of compressive strength. Calibration of hardening parameters can then enable capturing the nonlinear reduction in stiffness at increasing strain levels.

Authorship statement (CRediT)

Marialuigia Sangirardi: Conceptualisation, Methodology, Validation, Formal analysis, Investigation, Data Curation, Writing – Original Draft, Writing – Review & Editing, Visualisation. **Miles R.W. Judd**: Conceptualisation, Methodology, Validation, Formal analysis, Investigation, Data Curation, Writing – Original Draft, Writing – Review & Editing, Visualisation. **Anil Ozdemir**: Writing – Review & Editing. **Sinan Acikgoz**: Conceptualisation, Resources, Writing – Review & Editing, Supervision, Project Administration, Funding acquisition.

Acknowledgments

This work was carried out as a part of the "MINT – Masonry in-situ testing and material identification" project, supported by EPSRC (Grant Reference: EP/V048082/1). The authors are grateful to the anonymous reviewer for their suggestions, which helped improve the paper.

References

[1] BS EN 14580-2005. Natural stone test methods. Determination of static elastic modulus 2005.
[2] BS EN 12390-13. Testing hardened concrete. Part 13: Determination of secant modulus of elasticity in compression. n.d.
[3] BS 1881-209:1990. Testing concrete. Recommendations for the measurement of dynamic modulus of elasticity. 1990.
[4] BS EN 14146:2004. Natural stone test methods. Determination of the dynamic elastic modulus of elasticity (by measuring the fundamental resonance frequency). 2004.
[5] ASTM E1876-22. Test Method for Dynamic Youngs Modulus, Shear Modulus, and Poissons Ratio by Impulse Excitation of Vibration 2022.
[6] Ozdemir A, Sangirardi M, Judd M, Acikgoz S. Evaluation of test procedures and correlations for the mechanical characterisation of brick masonry and its constituents. Constr Build Mater 2025;489:142133. https://doi.org/10.1016/j.conbuildmat.2025.142133
[7] Kaklis K, Agioutantis Z, Mavrigiannakis S, Maravelaki-Kalaitzaki P. A simplified damage evolution relationship and deformation characteristics of a pozzolanic lime mortar when subjected to unloading-reloading cycles in the pre-peak region. Fract Struct Integr 2019;13:395-406. https://doi.org/10.3221/IGF-ESIS.50.33
[8] Patterson R, Pavía S. Influence of loading rate and specimen geometry on lime mortar strength. Bridge Infrastruct Concr Res Irel BCRI Dublin 2012:361-5.
[9] Zhang X, Garijo L, Ruiz G, Ortega JJ. Influence of loading rate on the fracture behaviour of natural hydraulic and aerial lime mortars. Proc 10th Int Conf Fract. Mech. Concr. Concr. Struct., 2019, p. 1-5. https://doi.org/10.21012/FC10.233356
[10] Hao H, Tarasov B. Experimental study of dynamic material properties of clay brick and mortar at different strain rates. Aust J Struct Eng 2008;8:117-32. https://doi.org/10.1080/13287982.2008.11464992
[11] Ciccotti M, Mulargia F. Differences between static and dynamic elastic moduli of a typical seismogenic rock. Geophys J Int 2004;157:474-7. https://doi.org/10.1111/j.1365-246X.2004.02213.x
[12] Zhang, Y., Gu, Y., Zhou, H., Yang, L., 2024. Extracting static elastic moduli of rock through elastic wave velocities. Acta Geophysica 72, 915-931 https://doi.org/10.1007/s11600-023-01139-9
[13] Bastgen K, Hermann V. Experience made in determining the static modulus of elasticity of concrete. Matér Constr 1977;10:357-64. https://doi.org/10.1007/BF02473733
[14] Neville AM. Properties of concrete. Wiley; 1973.
[15] Arca Y, Kurnaz K, Ispir M, Acikgoz S, Ersan Erus HO, Lava P, Ozdemir A. Post-Earthquake Characterisation of Building Stones Used in Hatay. Available SSRN 5293105 n.d.
[16] Eissa E, Kazi A. Relation between static and dynamic Young's moduli of rocks. Int J Rock Mech Min Geomech Abstr 1988;25. https://doi.org/10.1016/0148-9062(88)90987-4
[17] Makoond N, Cabané A, Pelà L, Molins C. Relationship between the static and dynamic elastic modulus of brick masonry constituents. Constr Build Mater 2020;259:120386. https://doi.org/10.1016/j.conbuildmat.2020.120386
[18] Marques AI, Morais J, Morais P, do Rosário Veiga M, Santos C, Candeias P, Ferreira JG. Modulus of elasticity of mortars: Static and dynamic analyses. Constr Build Mater 2020;232:117216. https://doi.org/10.1016/j.conbuildmat.2019.117216
[19] Saint-Astier NHL 3.5 - Technical Data Sheet. https://www.saint-astier.com/app/uploads/sites/2/2021/12/ASTIER-TDS-NHL35-EN-3P-23346-WEB.pdf Last accessed 25/04/2025 n.d.
[20] Drysdale RG, Hamid AA. Behavior of concrete block masonry under axial compression. J. Proc., vol. 76, 1979, p. 707-22. https://doi.org/10.14359/6965
[21] BS EN 1015-3:1999. Methods of test for mortar for masonry. Determination of consistence of fresh mortar (by flow table). 1999.
[22] Judd MRW, Wilson R, Sangirardi M, Pulatsu B, Acikgoz S. Experimental Characterisation of Hydraulic Lime Mortar and Clay Brick Elasticity using the Virtual Fields Method. Available SSRN 5203600 2025. https://doi.org/10.2139/ssrn.5203600
[23] Grassl P, Jirásek M. Damage-plastic model for concrete failure. Int J Solids Struct 2006;43:7166-96. https://doi.org/10.1016/j.ijsolstr.2006.06.032